Molecular Therapy
Methods & Clinical Development
Original Article

Ad- and AAV8-mediated *ABCA1* gene therapy in a murine model with retinal ischemia/reperfusion injuries

Jing Luo,[1] Shengli Wang,[1] Zhenlong Zhou,[1] and Yin Zhao[2]

[1]The First Affiliated Hospital, Biomedical Translational Research Institute and School of Pharmacy, Jinan University, Guangzhou 510632, China; [2]Department of Ophthalmology, Tongji Hospital, Tongji Medical College, Huazhong University of Science and Technology, Wuhan 430030, China

The anti-inflammatory molecule annexin A1 (ANXA1) determines the ultimate fate of retinal ganglion cell (RGC) in glaucoma. Cytoplasmic and extracellular ANXA1 facilitate resolution of inflammation. However, the nuclear translocation of ANXA1 induces RGC apoptosis in a murine glaucoma model, and the maintenance of ANXA1 secreted in the extracellular environments remains unclear. In this study, we found that intravitreal injection of the recombinant adenovirus vector (Ad)-ATP-binding cassette transporter A1 (*ABCA1*; carrying full-length *ABCA1*) improved RGC survival in the ischemia reperfusion (IR) mice model. Upregulation of ABCA1 maintained ANXA1 cytoplasmic location and reduced ANXA1 nuclear translocation, which is due to the decreased binding of ANXA1 with importin β. Moreover, we found that amino acids 903 to 1,344 of ABCA1 interacted with ANXA1 and decreased its nuclear localization. Importantly, intravitreal injection of adenovirus-associated viral (AAV) vector AAV8-*ABCA1* (carrying 903 to 1,344 fragments of ABCA1) maintained ANXA1 cytoplasmic location and improved RGC survival in the IR mice model. Thus, overexpression of *ABCA1* protects against RGC apoptosis by partially blocking ANXA1 nuclear translocation. This study puts forth a potential gene treatment strategy to prevent RGC apoptosis in glaucoma.

INTRODUCTION

Glaucoma, one of the severe causes of irreversible blindness worldwide, is characterized by the loss of retinal ganglion cells (RGCs).[1] Acute angle-closure glaucoma is an ocular emergency caused by a rapid increase in intraocular pressure (IOP).[2] One of the animal models that could mimic acute angle-closure glaucoma is the retinal ischemia reperfusion (IR) injury model.[3,4] Both ischemia and reperfusion processes contribute to RGC loss. In the IR model, rapid and transient elevation of IOP induces retinal ischemia and produces reactive oxygen species.[5,6]

Annexin A1 (ANXA1) is an anti-inflammatory molecule involved in inflammatory diseases.[7,8] The subcellular localization of ANXA1 determines cellular fate.[9] Following externalization, cytoplasmic ANXA1 interacts with its receptor *N*-formyl peptide receptor 2 (FPR2), which then activates downstream anti-inflammatory signaling to inhibit phospholipase A2.[10,11] However, the nuclear translocation of ANXA1 is associated with cancer progression via regulation of transcription factors and miRNAs.[12,13] In neuronal cells, the nuclear translocation of ANXA1 is associated with the induction of cellular apoptosis by regulating transcription factors, such as p53 and p65.[14,15] The maintenance of ANXA1 cytoplasmic localization is a critical factor in the RGC fate determination.

ATP-binding cassette (ABC) transporter A1 (ABCA1), a 254-kDa protein, was found associated with ANXA1 externalization.[16,17] The expression of ABCA1 was decreased in the IR mice model, and this protein was transcriptionally regulated by the liver X receptor (LXR). Our previous study demonstrated that the LXR agonist upregulated ABCA1 expression, promoted ANXA1 membrane translocation, and reduced RGC apoptosis.[18] In addition, the LXR agonist could protect against retinal damage in *N*-methyl-D-aspartate (NMDA) injury and an autoimmune uveitis animal model.[19] However, the mechanism of ABCA1-ANXA1 interactions and ABCA1-mediated ANXA1 subcellular localization is still unclear.

Adenovirus vectors (Ads) and adeno-associated virus (AAV) vectors are the most commonly used vectors for gene therapy.[20] However, AAV vectors are limited by their small packaging capacity (considered to be <5 kb). The human ABCA1 is 2,261 amino acids in length, which corresponds to more than 6.7 kb. In this study, we used Ad to carry full-length human *ABCA1* (Ad-*ABCA1*) and AAV to carry an *ABCA1* fragment to investigate the effect and mechanism of ABCA1 overexpression on ANXA1 subcellular localization.

RESULTS

Ad-*ABCA1* treatment reduced RGC loss in IR mice model

Intravitreal injection of the LXR agonist could upregulate ABCA1 expression and reduce RGC loss in the IR mice model.[18] To confirm

Received 2 August 2020; accepted 18 January 2021;
https://doi.org/10.1016/j.omtm.2021.01.012.

Correspondence: Yin Zhao, Department of Ophthalmology, Tongji Hospital, Tongji Medical College, Huazhong University of Science and Technology, Wuhan 430030, China.
E-mail: zhaoyin85@hust.edu.cn

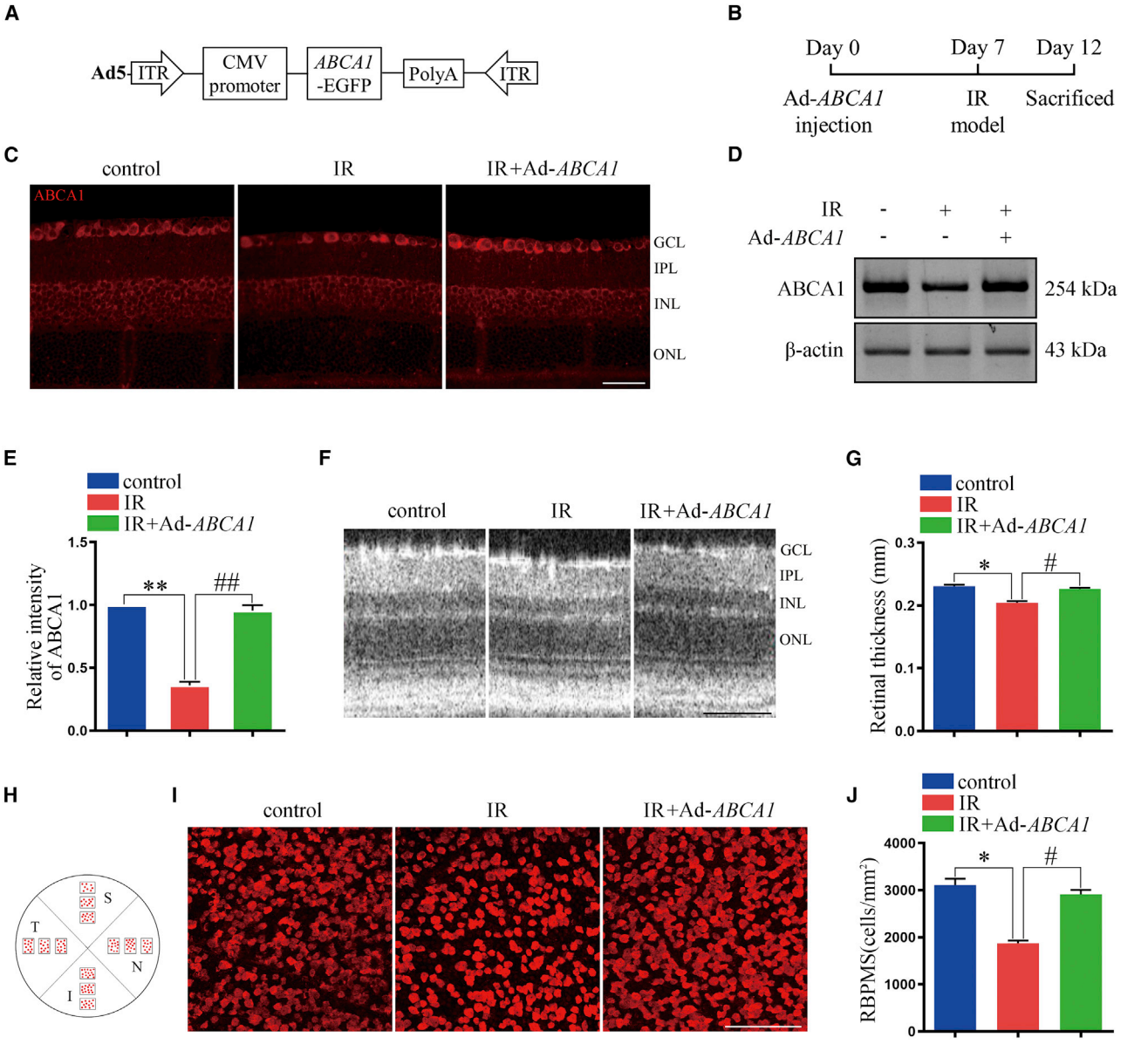

Figure 1. The effect of Ad-*ABCA1* overexpression on retina degeneration after IR *in vivo*

(A) Graphic illustration of the structure of Ad-*ABCA1*. (B) Experimental scheme of Ad-*ABCA1* administration and the mouse IR model. (C) Representative immunofluorescence images for ABCA1 expression in retina slices. Scale bar, 50 μm. (D) Western blot analysis showing the expression of ABCA1 in retina after Ad-*ABCA1* administration. These results are obtained from three independent experiments. (E) Statistical analysis of (D). **p < 0.01, compared with control retina; ##p < 0.01 compared with the IR group (n = 3 retinas per group). (F) Representative SD-OCT images for the thickness of the retina. Scale bar, 100 μm. GCL, ganglion cell layer; IPL, inner plexiform layer; INL, inner nuclear layer; and ONL, outer nuclear layer. (G) Statistical analysis of (F). *p < 0.05 compared with control retina; #p < 0.05 compared with the IR group (n = 8 retinas per group). (H) Graphic illustration of the RBPMS analysis. S, superior; N, nasal; I, inferior; and T, temporal. (I) Representative immunofluorescence results showing the number of retinal ganglion cell (RGC), n = 8 retinas per group. Scale bar, 100 μm. (J) Statistical analysis of (I). *p < 0.05, compared with control retina; #p < 0.05 compared with the IR group. All of the data are expressed as mean ± SEM, one-way ANOVA followed by a Tukey's post hoc test.

the effect of ABCA1 overexpression on RGC apoptosis, Ad-*ABCA1* and immunofluorescence (IF) staining were used to examine the expression of ABCA1 in the retina. We found that compared with the IR group, the expression of ABCA1 was increased in the Ad-*ABCA1* group (Figure 1C). The expression of ABCA1 in retina extract was increased in the Ad-*ABCA1* group (Figures 1D and 1E). qPCR results also confirmed that Ad-*ABCA1* could increase *ABCA1* mRNA expression (Figure S2B). In Figures S3A and S3B, we have presented the GFP images from an Ad-*ABCA1*-infected retina. We used spectral-domain optical coherence tomography (SD-OCT) to examine

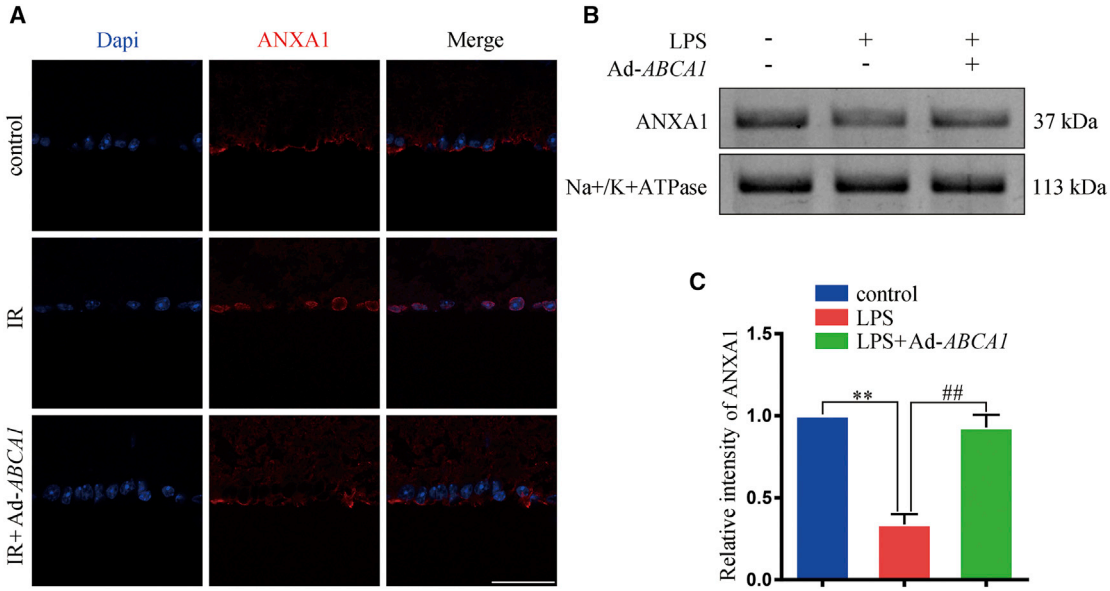

Figure 2. The effect of Ad-*ABCA1* overexpression on ANXA1 nuclear localization *in vivo* and *in vitro*

(A) Representative immunofluorescence images of ANXA1 expression on the retinal GCL, n = 4 retinas per group. Scale bar, 50 μm. (B) Western blot analysis showing the expression of ANXA1 in cellular membrane extract in HEK293 cells. (C) Statistical analysis of (B); the data of three independent experiments expressed as the mean ± SD. **p < 0.01, compared with control; ##p < 0.01 compared with the LPS group, one-way ANOVA with Bonferroni post hoc test.

the morphological changes in the retina *in vivo*. As shown in Figures 1F and 1G, after IR, the thickness of the retina decreased, whereas after Ad-*ABCA1* treatment, the retina exhibited sufficient thickness. Most importantly, retinal whole-mount immunostaining with RNA-binding protein with multiple splicing (RBPMS) showed that the RGC number in the IR group decreased, and Ad-*ABCA1* treatment could reverse this reduction (Figures 1H–1J).

Ad-*ABCA1* treatment maintained ANXA1 membrane translocation after IR

Previous studies found ABCA1 to be associated with ANXA1 externalization.[16,17] To investigate the effect of ABCA1 overexpression on ANXA1 subcellular localization, immunostaining was performed on retina slices to examine the expression of ANXA1. As shown in Figure 2A, IR induced ANXA1 nuclear localization, visualized using 4′,6-diamidino-2-phenylindole (DAPI), whereas treating with Ad-*ABCA1*, decreased ANXA1 nuclear translocation. We also examined ANXA1 expression in the cellular membrane extract. In Figures 2B and 2C, we found that lipopolysaccharide (LPS) treatment decreased ANXA1 expression, whereas Ad-*ABCA1* maintained ANXA1 expression in membrane extract in HEK293 cells.

ABCA1 decreased ANXA1 nuclear translocation by competing with importin β

Previous studies found that ANXA1 nuclear translocation was associated with importin β;[15,21,22] however, whether the decrease in ANXA1 nuclear translocation associated with ABCA1 overexpression was due to competition with importin β remained unclear. Here, we used Ad-*ABCA1* and *ABCA1* small interfering RNA (siRNA) to upregulate (Figure S2A) and downregulate (Figures S2D–S2F) ABCA1 expression, respectively. We found that in HEK239 cells, LPS induced ANXA1 nuclear translocation, which could be partially blocked by Ad-*ABCA1* (Figures 3A and 3B). We further found that Ad-*ABCA1* could decrease binding of ANXA1 with importin β (Figure 3C). We also found that decreased ABCA1 expression could increase binding of ANXA1 with importin β (Figure 3D). In addition, we used the importin β1-specific inhibitor importazole (IPZ) to block the importin β function. We found that *ABCA1* siRNA increased ANXA1 nuclear localization, whereas IPZ could partially block its effect (Figures 3E and 3F).

ABCA1 interacted with ANXA1

The structure of ABCA1 has been recently reported.[23] This protein mainly contains two transmembrane domains, two extracellular domain, and two main intracellular domains (Figure 4A). Each intracellular domain contains one intracellular helix, one nucleotide-binding domain, and one regulatory domain. Here, we constructed two plasmids containing ABCA1 intracellular domains (amino acids 903 to 1,344 and amino acids 1,907 to 2,220). Coimmunoprecipitation results showed that the amino acids 903 to 1,344 fragment of ABCA1 interacted with ANXA1 (Figure 4B). In addition, we transfected HEK293 cells with a plasmid containing the ABCA1 903–1,344 fragment and found that the expression of ANXA1 was increased in the membrane extract and decreased in the nuclear extract (Figures 4C and 4D). These results indicate that the amino acids 903–1,344 fragment of ABCA1 contains the domain that binds with ANXA1 and maintains ANXA1 membrane localization.

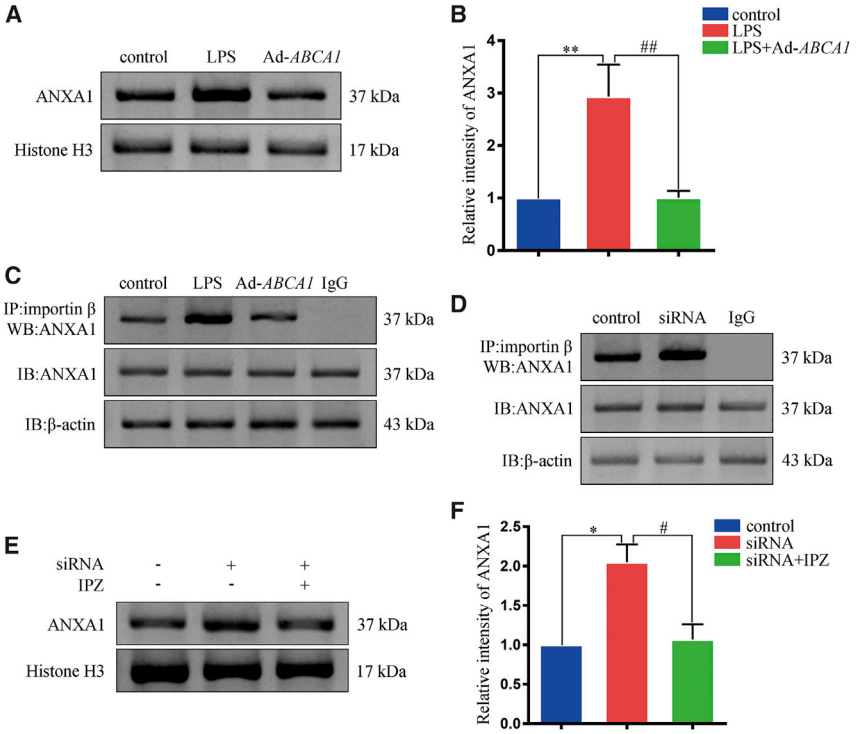

Figure 3. The mechanism of *ABCA1* overexpression on ANXA1 nuclear localization

(A) Western blot analysis showing the expression of ANXA1 in the cellular nuclear extract in HEK293 cells. (B) Statistical analysis of (A). **p < 0.01, compared with control; ##p < 0.01 compared with the LPS group. (C) A western blotting analysis indicates that LPS induces the interaction between importin β and ANXA1, and this effect is inhibited by Ad-*ABCA1* treatment. IP, immunoprecipitation; IB, immunoblotting; and WB, western blot. (D) A western blotting analysis indicates that *ABCA1* siRNA induces the interaction between importin β and ANXA1. (E) Western blot analysis showing the expression of ANXA1 in the cellular nuclear extract in HEK293 cells. IPZ, importazole. (F) Statistical analysis of (E). *p < 0.05, compared with controls; #p < 0.05 compared with the *ABCA1* siRNA group. All of the data of the three independent experiments are expressed as the mean ± SD, one-way ANOVA with Bonferroni post hoc test.

AAV8-*ABCA1* (903–1,344) pretreatment decreased ANXA1 nuclear translocation after IR

To assess the impact of ABCA1 amino acids 903–1,344 on ANXA1 nuclear localization *in vivo*, we used AAV8-*ABCA1* (903–1,344) and examined the expression of ANXA1 using retinal slices. The qPCR results revealed that AAV8-*ABCA1* (903–1,344) could upregulate ABCA1 (fragment 903–1,344) mRNA expression (Figure S2C). The AAV8-*ABCA1* (903–1,344) pretreatment group showed less nuclear staining upon general observation (Figure 5C).

AAV8-*ABCA1* (903–1,344) pretreatment reduced RGC loss after IR

To confirm the treatment effect of AAV8-*ABCA1* (903–1,344) on RGC apoptosis after IR, we performed SD-OCT to examine the morphological changes in the retina *in vivo*. We found that AAV8-*ABCA1* (903–1,344) pretreatment could reduce retina degeneration after IR (Figures 6A and 6B). Furthermore, we found that AAV8-*ABCA1* (903–1,344) pretreatment could reverse RGC loss after IR (Figures 6C and 6D). However, AAV8-*ABCA1* (1,907–2,220)

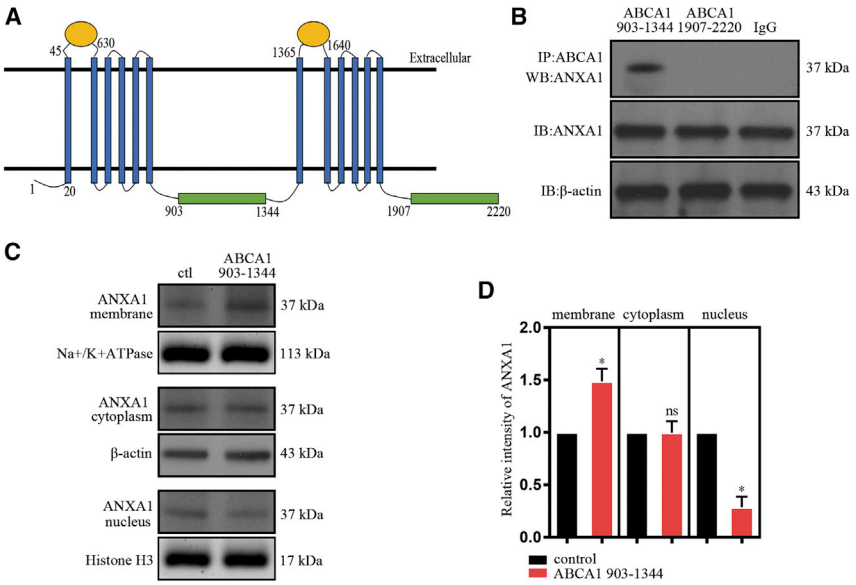

Figure 4. The interaction between ABCA1 and ANXA1

(A) Schematic diagram of full-length ABCA1. (B) A western blotting analysis is showing the interaction between the 903−1,344 fragment and the 1,907−2,220 fragment of ABCA1 and ANXA1. (C) Western blot analysis showing the expression of ANXA1 in membrane, cytoplasm, and nucleus extract after ABCA1 903−1,344 fragment overexpression. (D) Statistical analysis of (C); the data of three independent experiments expressed as the mean ± SD. *p < 0.05, unpaired Student's t test versus control.

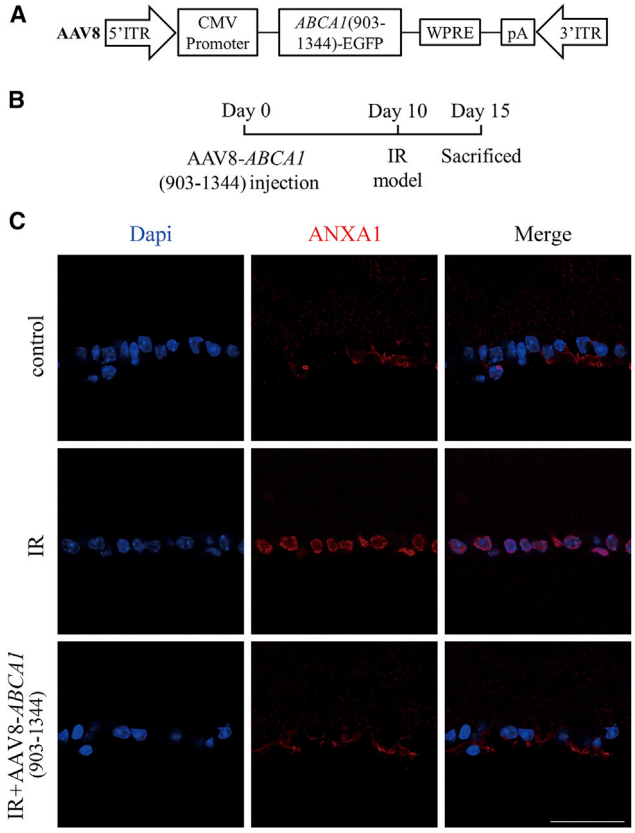

Figure 5. The effect of AAV8-*ABCA1* (903–1,344) overexpression on ANXA1 nuclear localization after IR *in vivo*

(A) Graphic illustration of the structure of AAV8-*ABCA1* (903−1,344). (B) Experimental scheme of AAV8-*ABCA1* (903−1,344) administration and the mouse IR model. (C) Representative immunofluorescence images of ANXA1 expression on retina GCL, n = 4 retinas per group. Scale bar, 50 μm.

injection could not reverse retina degeneration or RGC apoptosis (Figures S1A and S1B). We also examined the effect of AAV8-*ABCA1* (903–1,344) post-treatment on retina degeneration and RGC apoptosis. We found that AAV8-*ABCA1* (903–1,344) post-treatment could not improve retina degeneration or RGC apoptosis after IR (Figures S1D−S1F). Similarly, an AAV empty vector could not reverse retina degeneration after IR (Figure S1C).

DISCUSSION

This study demonstrated that *ABCA1* overexpression decreased ANXA1 nuclear translocation *in vivo* and *in vitro* and mitigated retina degeneration and RGC loss after IR. These results suggest that ABCA1 or/and ANXA1 could be considered as a gene therapy target for glaucoma disease.

ANXA1 subcellular localization determines cellular fate. In inflammatory diseases and the immune response system, treatment with exogenous ANXA1 mimetic peptides can decrease the expression of proinflammatory mediators, attenuating the infiltration of inflammatory cells.[24] By interacting with FPR2, ANXA1 can also limit viral replication in the influenza A virus infection model.[25] Extracellular ANXA1 promotes stem cell differentiation[26] and reduces cancer cell growth and aggressiveness.[27] However, ANXA1 nuclear translocation induces cellular apoptosis by interacting with p53 and p65. In this study, we found that *ABCA1* overexpression could promote RGC survival in an IR mouse model. We speculated that overexpression of full-length ABCA and its amino acids 903–1,344 fragment promoted the RGC survival rate by reducing ANXA1 nuclear localization.

Previous studies have reported that ABCA1 could interact with ANXA1 and induce externalization of ANXA1. However, the underlying mechanism remains unclear. S100A11 is another protein reported to be an ANXA1 nuclear translocation regulator. S100A11 overexpression can downregulate ANXA1 binding with importin β, which partially interferes with ANXA1 nuclear translocation.[28] Similarly, in this study, we found that ABCA1 overexpression could reduce ANXA1 binding with importin β and decrease ANXA1 nuclear localization. Moreover, we found that the amino acids 903–1,344 fragment of ABCA1 interacted with ANXA1 and could be considered a key domain for the ABCA1-ANXA1 interaction. We speculated that ABCA1 reduced ANXA1 nuclear translocation by decreasing ANXA1 binding with importin β, which indicated that ABCA1 was competitively binding with ANXA1 and reducing ANXA1 nuclear translocation. However, whether importin β can proactively and specifically transport ANXA1 into the nucleus and reduce ABCA1–ANXA1 binding remains unclear.

The structure of human ABCA1 was recently identified.[23] We speculated that ABCA1 binding with ANXA1 occurred on its intracellular domain. Coimmunoprecipitation results also identified that the intracellular domain of ABCA1 (amino acids 903–1,344 fragment) could bind with ANXA1. The ABCA1 fragment (amino acids 1,907–2,220) could not bind with ANXA1 or reverse retina degeneration. We assumed that this is due to the presence of the unconjugated form of ANXA1. A limitation of this study was that the amino acids 903–1,344 fragment of ABCA1 contained three functional domains, including one nucleotide-binding domain, one regulatory domain, and one intracellular helices domain. Further studies should identify which domain of this fragment could specifically bind with ANXA1. Further, more studies are needed to identify other structures in ABCA1 that could potentially interact with ANXA1, such as two transmembrane domains and two extracellular domains. Another limitation of this study is that the adenovirus injection might have activated the immune system, including the Toll-like receptor (TLR)-dependent and TLR-independent pathways. More studies are warranted to silence retinal microglia and thereafter investigate the function of Ad-*ABCA1* on retina degeneration.

Our findings identify a novel treatment strategy for RGC loss in the IR mice model. Overexpression of the full-length and amino acids 903–1,344 fragment of *ABCA1* decreased ANXA1 nuclear localization.

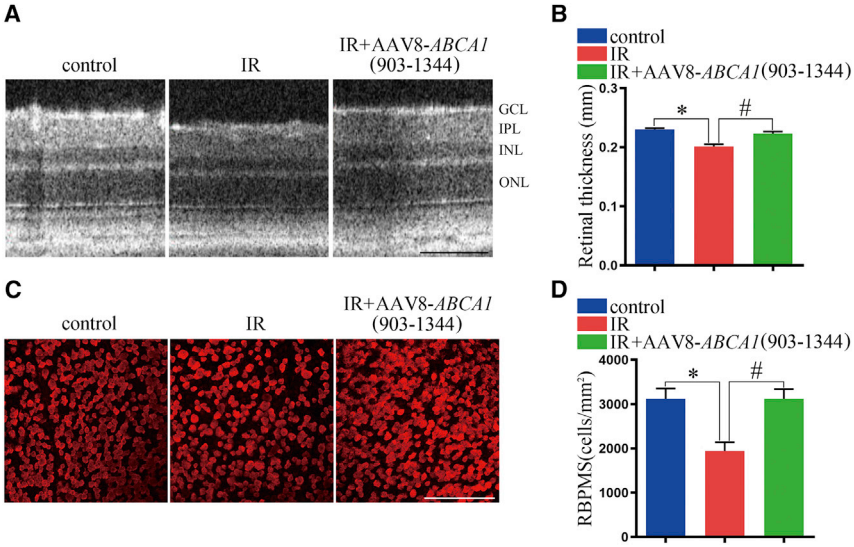

Figure 6. The effect of AAV8-*ABCA1* (903–1,344) overexpression on retina degeneration after IR *in vivo*

(A) Representative SD-OCT images for the thickness of the retina (n = 8 retinas per group). Scale bar, 100 μm. (B) Statistical analysis of (A). *p < 0.05 compared with control retina; #p < 0.05 compared with the IR group. (C) Representative immunofluorescence results showing the number of RGCs, n = 8 retinas per group. Scale bar, 100 μm. (D) Statistical analysis of (C). *p < 0.05, compared with control retina; #p < 0.05 compared with the IR group. All of the data are expressed as mean ± SEM, one-way ANOVA followed by Tukey's post hoc test.

The reduced RGC loss associated with ABCA1 overexpression was brought about due to interference of the ANXA1-importin β interaction and maintenance of ANXA1 membrane localization. These findings reveal ABCA1 and ANXA1 as novel targets for glaucoma gene therapies.

MATERIALS AND METHODS

Animals

Male C57BL/6J mice (3 months old, 20–25 g) were obtained from the Experiment Animal Center of Tongji Medical College. All of the mice were fed with a standard rodent diet *ad libitum* and kept on a 12-h light/12-h dark cycle. The procedures concerning animals were performed according to the Association for Research in Vision and Ophthalmology statement for the Use of Animals in Ophthalmic and Vision Research and under protocols approved by the Institutional Animal Care and Use Committees at Huazhong University of Science and Technology (HUST; 2015-K-023).

Reagents and antibodies

IPZ was obtained was from Calbiochem (Darmstadt, Germany; 401105, 8 μM). Human *ABCA1 siRNA* was obtained from Thermo Fisher Scientific (Shanghai, China; assay ID 107728, catalog #AM16708).

The following antibodies were used in this study: anti-ABCA1 (ab-18180, Research Resource Identifier [RRID]: AB_444302; Abcam; 1:500 for western blot, 1:200 for IF), anti-ANXA1 (ab-214486; Abcam; 1:2,000 for western blot, 1:1,000 for IF), anti-RBPMS (ABN1362; Millipore; 1:500), anti-β-actin (sc-47778, RRID: AB_2714189; Santa Cruz; 1:1,000), anti-importin β (#51186, RRID: AB_2799386; Cell Signaling Technology; 1:1,000), anti-beta 1 sodium potassium ATPase (ab-2873, RRID: AB_303375; Abcam; 1:250), and anti-histone H3 (#4499, RRID: AB_10544537; Cell Signaling Technology; 1:1,000).

Intravitreal injections

The Ad-*ABCA1* gene (1×10^{11} viral genomes/mL) and AAV-encompassing amino acids 903–1,344 fragment of *ABCA1* (AAV8-*ABCA1* 903−1,344; 1×10^{12} viral genomes/mL) were obtained from BrainVTA (Wuhan, China). The experimental eyes were injected with Ad-*ABCA1* (1.5 μL) and AAV8-*ABCA1* 903–1,344 (1.5 μL) into the vitreous cavity through a 35G needle with a 10-μL Hamilton micro syringe (Hamilton, Reno, NV, USA) before the onset of reperfusion at 7 days and 10 days, respectively. Tobramycin was applied to prevent bacterial infection.

IR mouse model

Mice were dark adapted overnight and anesthetized with an intraperitoneal injection of ketamine (15 mg/g body weight) and xylazine (7 mg/g). Their right eyes were dilated with 5% tropicamide, followed by topical anesthesia using proparacaine. We inserted a 30G needle into the anterior chamber (right eyes); the needle was connected to a saline reservoir. We elevated the saline reservoir to keep the IOP at 75 mmHg for 45 min. Retinal ischemia was confirmed by whitening of the iris. Then, we withdrew the needle and treated the mice with tobramycin to avoid bacterial infection. We kept the left eyes as control. All mice were sacrificed 120 h after this surgery.

Retinal thickness measurement *in vivo*

Retina thickness was measured by SD-OCT using the Spectralis HRA+OCT system (Heidelberg Engineering). Mice were anesthetized by intraperitoneal injection of ketamine (15 mg/g body weight) and xylazine (7 mg/g). Pupils were dilated with drops of Tropicamide Ophthalmic Solution USP 1% (Bausch & Lomb). An artificial tear was applied bilaterally to prevent corneal dehydration during the procedure. Total retinal thickness was defined as the width from the inner-limiting membrane to the retinal pigment epithelium (RPE)/choroid layer on the cross-sectional images and measured using custom-automated image segmentation routines in MATLAB.

IF

We washed 5 μm paraffin-embedded retinal sections twice with phosphate-buffered saline (PBS; at 37°C). Afterward, the sections were incubated with 5% bovine serum albumin (BSA) for 1 h and were then treated with mouse monoclonal ABCA1 antibody and rabbit monoclonal ANXA1 antibody in 5% BSA at 4°C overnight. Retinal sections were then washed and treated with secondary antibody (1:200; Invitrogen) in 5% BSA at 37°C for 1 h. A Zeiss confocal microscope was used to acquire fluorescence images (Zeiss LSM 700; Germany).

Coimmunoprecipitation

We used a buffer containing 400 mM KCl, 20 mM 4-(2-hydroxyethyl)-1-piperazineethanesulfonic acid, 5 mM ethylenediaminetetraacetic acid, 0.4% NP-40, protease inhibitors, and 5% glycerol to obtain cell lysates by sonication. We incubated the cell lysates with an anti-importin β antibody overnight at 4°C. Then, we used protein A/G PLUS-Agarose beads (sc-2003; Santa Cruz) to incubate the reaction mixture for 2 h at 4°C. The precipitates were then washed three times with a washing buffer and eluted from the beads by boiling with 1 × sodium dodecyl sulfate (SDS) for 5 min at 95°C. The protein samples were detected by SDS-polyacrylamide gel electrophoresis.

Protein extraction and preparation

We prepared the protein samples using the Membrane and Cytosol Protein Extraction Kit (P0033; Beyotime, China). In brief, we washed the HEK293 cells with ice-cold PBS and harvested the cells using a cell scraper. The cells were centrifuged at 3,000 × *g* for 5 min. We then resuspended the cell pellets in a membrane and cytoplasmic extraction buffer that contained protease inhibitors and phenylmethanesulfonyl fluoride. The cell pellets were placed on ice with the extraction buffer for 30 min, and the lysates were then centrifuged at 12,000 × *g* at 4°C for 10 min. The membrane-bound and cytoplasmic protein fractions were harvested for expression analysis, which was performed later.

We used ImageJ (Fiji) to detect the western blotting bands and performed a band density analysis.

Statistical analysis

We used GraphPad Prism software (version 5.0; GraphPad Software) to perform the statistical analysis. Data were analyzed using Student's t test and a one-way analysis of variance (ANOVA) to determine statistically significant differences. A value of $p < 0.05$ was considered statistically significant.

SUPPLEMENTAL INFORMATION

Supplemental Information can be found online at https://doi.org/10.1016/j.omtm.2021.01.012.

ACKNOWLEDGMENTS

The current studies were supported by funding from the National Natural Science Foundation of China grant no. 31800868 and Tongji Hospital (HUST) Foundation for Excellent Young Scientist grant no. 2020YQ18 (to Y.Z.); and National Natural Science Foundation of China grant no. 31900657, the China Postdoctoral Science Foundation grant nos. 2018M643375 and 2020T130251, and the Postdoctoral Fund of the First Affiliated Hospital, Jinan University grant no. 801323 (to J.L.).

AUTHOR CONTRIBUTIONS

Y.Z. conceived and designed the project and wrote the manuscript. J.L. performed the experiments. S.W. and Z.Z. helped to revise the manuscript.

DECLARATION OF INTERESTS

The authors declare no competing interests.

REFERENCES

1. Weinreb, R.N., Aung, T., and Medeiros, F.A. (2014). The pathophysiology and treatment of glaucoma: a review. JAMA *311*, 1901–1911.
2. Emanuel, M.E., Parrish, R.K., 2nd, and Gedde, S.J. (2014). Evidence-based management of primary angle closure glaucoma. Curr. Opin. Ophthalmol. *25*, 89–92.
3. Chi, W., Li, F., Chen, H., Wang, Y., Zhu, Y., Yang, X., Zhu, J., Wu, F., Ouyang, H., Ge, J., et al. (2014). Caspase-8 promotes NLRP1/NLRP3 inflammasome activation and IL-1β production in acute glaucoma. Proc. Natl. Acad. Sci. USA *111*, 11181–11186.
4. Huang, J., Zhao, Q., Li, M., Duan, Q., Zhao, Y., and Zhang, H. (2019). The effects of endothelium-specific CYP2J2 overexpression on the attenuation of retinal ganglion cell apoptosis in a glaucoma rat model. FASEB J. *33*, 11194–11209.
5. Minhas, G., Sharma, J., and Khan, N. (2016). Cellular Stress Response and Immune Signaling in Retinal Ischemia-Reperfusion Injury. Front. Immunol. *7*, 444.
6. Osborne, N.N., Casson, R.J., Wood, J.P., Chidlow, G., Graham, M., and Melena, J. (2004). Retinal ischemia: mechanisms of damage and potential therapeutic strategies. Prog. Retin. Eye Res. *23*, 91–147.
7. Purvis, G.S.D., Solito, E., and Thiemermann, C. (2019). Annexin-A1: Therapeutic Potential in Microvascular Disease. Front. Immunol. *10*, 938.
8. Gobbetti, T., and Cooray, S.N. (2016). Annexin A1 and resolution of inflammation: tissue repairing properties and signalling signature. Biol. Chem. *397*, 981–993.
9. Boudhraa, Z., Bouchon, B., Viallard, C., D'Incan, M., and Degoul, F. (2016). Annexin A1 localization and its relevance to cancer. Clin. Sci. (Lond.) *130*, 205–220.
10. Parente, L., and Solito, E. (2004). Annexin 1: more than an anti-phospholipase protein. Inflamm. Res. *53*, 125–132.
11. Girol, A.P., Mimura, K.K.O., Drewes, C.C., Bolonheis, S.M., Solito, E., Farsky, S.H.P., Gil, C.D., and Oliani, S.M. (2013). Anti-inflammatory mechanisms of the annexin A1 protein and its mimetic peptide Ac2-26 in models of ocular inflammation in vivo and in vitro. J. Immunol. *190*, 5689–5701.
12. Yuan, Y., Anbalagan, D., Lee, L.H., Samy, R.P., Shanmugam, M.K., Kumar, A.P., Sethi, G., Lobie, P.E., and Lim, L.H.K. (2016). ANXA1 inhibits miRNA-196a in a negative feedback loop through NF-kB and c-Myc to reduce breast cancer proliferation. Oncotarget *7*, 27007–27020.
13. Anbalagan, D., Yap, G., Yuan, Y., Pandey, V.K., Lau, W.H., Arora, S., Bist, P., Wong, J.S.B., Sethi, G., Nissom, P.M., et al. (2014). Annexin-A1 regulates microRNA-26b* and microRNA-562 to directly target NF-κB and angiogenesis in breast cancer cells. PLoS ONE *9*, e114507.
14. Zhao, Y., Li, X., Gong, J., Li, L., Chen, L., Zheng, L., Chen, Z., Shi, J., and Zhang, H. (2017). Annexin A1 nuclear translocation induces retinal ganglion cell apoptosis after ischemia-reperfusion injury through the p65/IL-1beta pathway. Biochim. Biophys. Acta Mol. Basis Dis. *1863*, 1350–1358.
15. Li, X., Zhao, Y., Xia, Q., Zheng, L., Liu, L., Zhao, B., and Shi, J. (2016). Nuclear translocation of annexin 1 following oxygen-glucose deprivation-reperfusion induces apoptosis by regulating Bid expression via p53 binding. Cell Death Dis. *7*, e2356.
16. Chapman, L.P., Epton, M.J., Buckingham, J.C., Morris, J.F., and Christian, H.C. (2003). Evidence for a role of the adenosine 5′-triphosphate-binding cassette

transporter A1 in the externalization of annexin I from pituitary folliculo-stellate cells. Endocrinology *144*, 1062–1073.

17. Omer, S., Meredith, D., Morris, J.F., and Christian, H.C. (2006). Evidence for the role of adenosine 5′-triphosphate-binding cassette (ABC)-A1 in the externalization of annexin 1 from pituitary folliculostellate cells and ABCA1-transfected cell models. Endocrinology *147*, 3219–3227.

18. Li, L., Xu, L., Chen, W., Li, X., Xia, Q., Zheng, L., Duan, Q., Zhang, H., and Zhao, Y. (2018). Reduced Annexin A1 Secretion by ABCA1 Causes Retinal Inflammation and Ganglion Cell Apoptosis in a Murine Glaucoma Model. Front. Cell. Neurosci. *12*, 347.

19. Zheng, S., Yang, H., Chen, Z., Zheng, C., Lei, C., and Lei, B. (2015). Activation of liver X receptor protects inner retinal damage induced by N-methyl-D-aspartate. Invest. Ophthalmol. Vis. Sci. *56*, 1168–1180.

20. Chen, Y.H., Keiser, M.S., and Davidson, B.L. (2018). Viral Vectors for Gene Transfer. Curr. Protoc. Mouse Biol. *8*, e58.

21. Zhao, Y., Wang, J., Jiang, H., Yu, Z., Li, X., and Shi, J. (2015). Following OGD/R, annexin 1 nuclear translocation and subsequent induction of apoptosis in neurons are assisted by myosin IIA in a TRPM7 kinase-dependent manner. Mol. Neurobiol. *51*, 729–742.

22. Li, X., Zheng, L., Xia, Q., Liu, L., Mao, M., Zhou, H., Zhao, Y., and Shi, J. (2019). A novel cell-penetrating peptide protects against neuron apoptosis after cerebral ischemia by inhibiting the nuclear translocation of annexin A1. Cell Death Differ. *26*, 260–275.

23. Qian, H., Zhao, X., Cao, P., Lei, J., Yan, N., and Gong, X. (2017). Structure of the Human Lipid Exporter ABCA1. Cell *169*, 1228–1239.e10.

24. Liu, L., An, D., Xu, J., Shao, B., Li, X., and Shi, J. (2018). Ac2-26 Induces IKKβ Degradation Through Chaperone-Mediated Autophagy Via HSPB1 in NCM-Treated Microglia. Front. Mol. Neurosci. *11*, 76.

25. Schloer, S., Hübel, N., Masemann, D., Pajonczyk, D., Brunotte, L., Ehrhardt, C., Brandenburg, L.O., Ludwig, S., Gerke, V., and Rescher, U. (2019). The annexin A1/FPR2 signaling axis expands alveolar macrophages, limits viral replication, and attenuates pathogenesis in the murine influenza A virus infection model. FASEB J. *33*, 12188–12199.

26. Barbosa, C.M.V., Fock, R.A., Hastreiter, A.A., Reutelingsperger, C., Perretti, M., Paredes-Gamero, E.J., and Farsky, S.H.P. (2019). Extracellular annexin-A1 promotes myeloid/granulocytic differentiation of hematopoietic stem/progenitor cells via the Ca2+/MAPK signalling transduction pathway. Cell Death Discov. *5*, 135.

27. Vecchi, L., Alves Pereira Zóia, M., Goss Santos, T., de Oliveira Beserra, A., Colaço Ramos, C.M., França Matias Colombo, B., Paiva Maia, Y.C., Piana de Andrade, V., Teixeira Soares Mota, S., Gonçalves de Araújo, T., et al. (2018). Inhibition of the AnxA1/FPR1 autocrine axis reduces MDA-MB-231 breast cancer cell growth and aggressiveness in vitro and in vivo. Biochim. Biophys. Acta Mol. Cell Res. *1865*, 1368–1382.

28. Xia, Q., Li, X., Zhou, H., Zheng, L., and Shi, J. (2018). S100A11 protects against neuronal cell apoptosis induced by cerebral ischemia via inhibiting the nuclear translocation of annexin A1. Cell Death Dis. *9*, 657.

OMTM, Volume *20*

Supplemental Information

Ad- and AAV8-mediated *ABCA1* gene therapy in a murine model with retinal ischemia/reperfusion injuries

Jing Luo, Shengli Wang, Zhenlong Zhou, and Yin Zhao

Supplementary figure 1

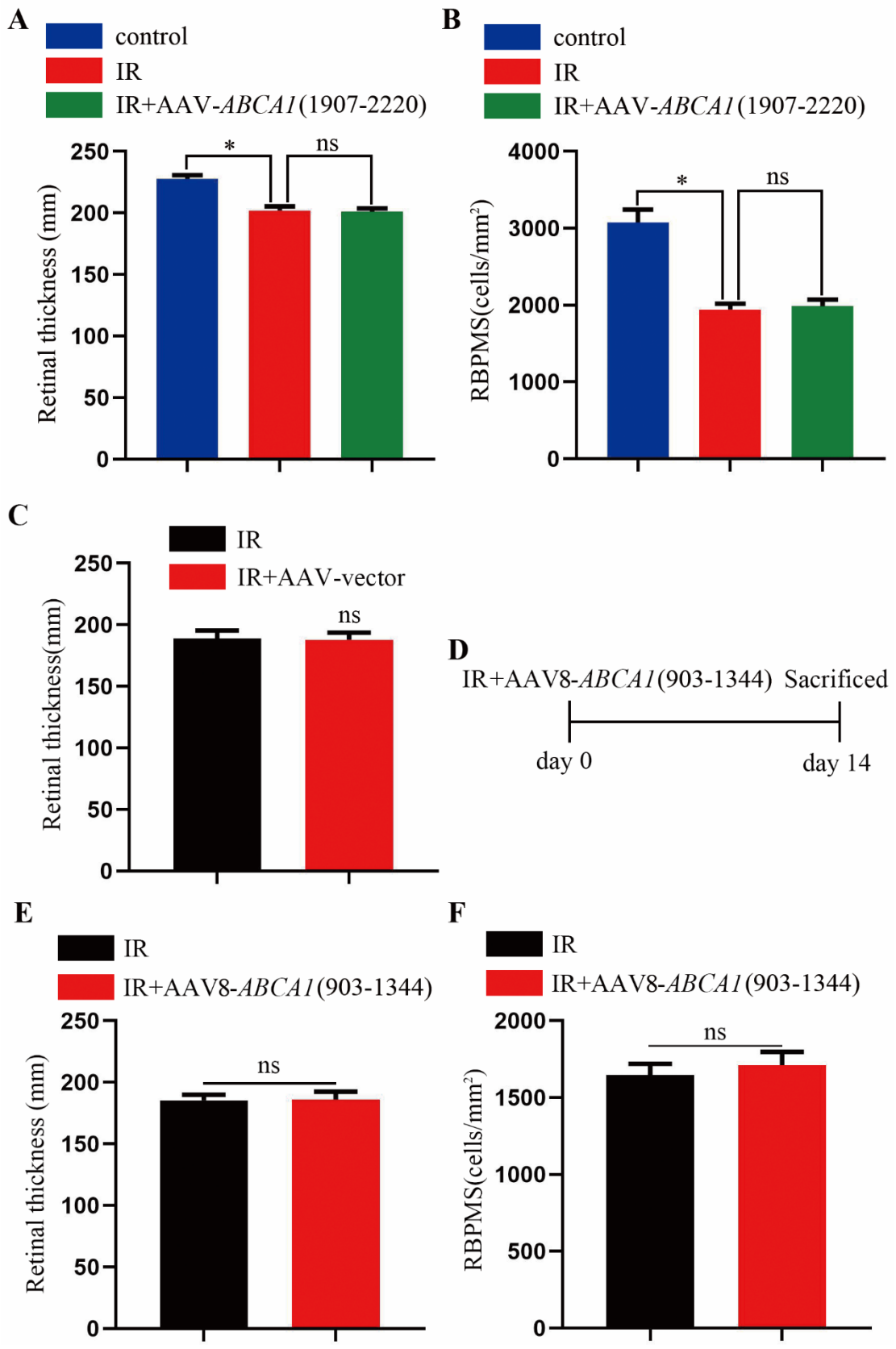

Supplementary figure 1 The effect of AAV8-ABCA1 on retina degeneration and RGC loss after IR. (A) Statistical analysis of SD-OCT results for mice retinal thickness.

The data are expressed as mean ±S.E.M. (n = 8 retinas per group). *P < 0.05 compared with control retina, one-way ANOVA followed by Tukey's post hoc test. (B) Statistical analysis of RGC number. The data are expressed as mean ±S.E.M. (n = 8 retinas per group). *P < 0.05 compared with control retina, one-way ANOVA followed by Tukey's post hoc test. (C) Statistical analysis of SD-OCT results for mice retinal thickness. The data are expressed as mean ±S.E.M. (n = 8 retinas per group), unpaired Student's t-test vs IR group. (D) Experimental scheme of AAV8-ABCA1 administration and mice IR model. (E) Statistical analysis of SD-OCT results for mice retinal thickness. The data are expressed as mean ±S.E.M. (n = 8 retinas per group), unpaired Student's t-test vs IR group. (F) Statistical analysis of RGC number. The data are expressed as mean ±S.E.M. (n = 8 retinas per group), unpaired Student's t-test vs IR group.

Supplementary figure 2

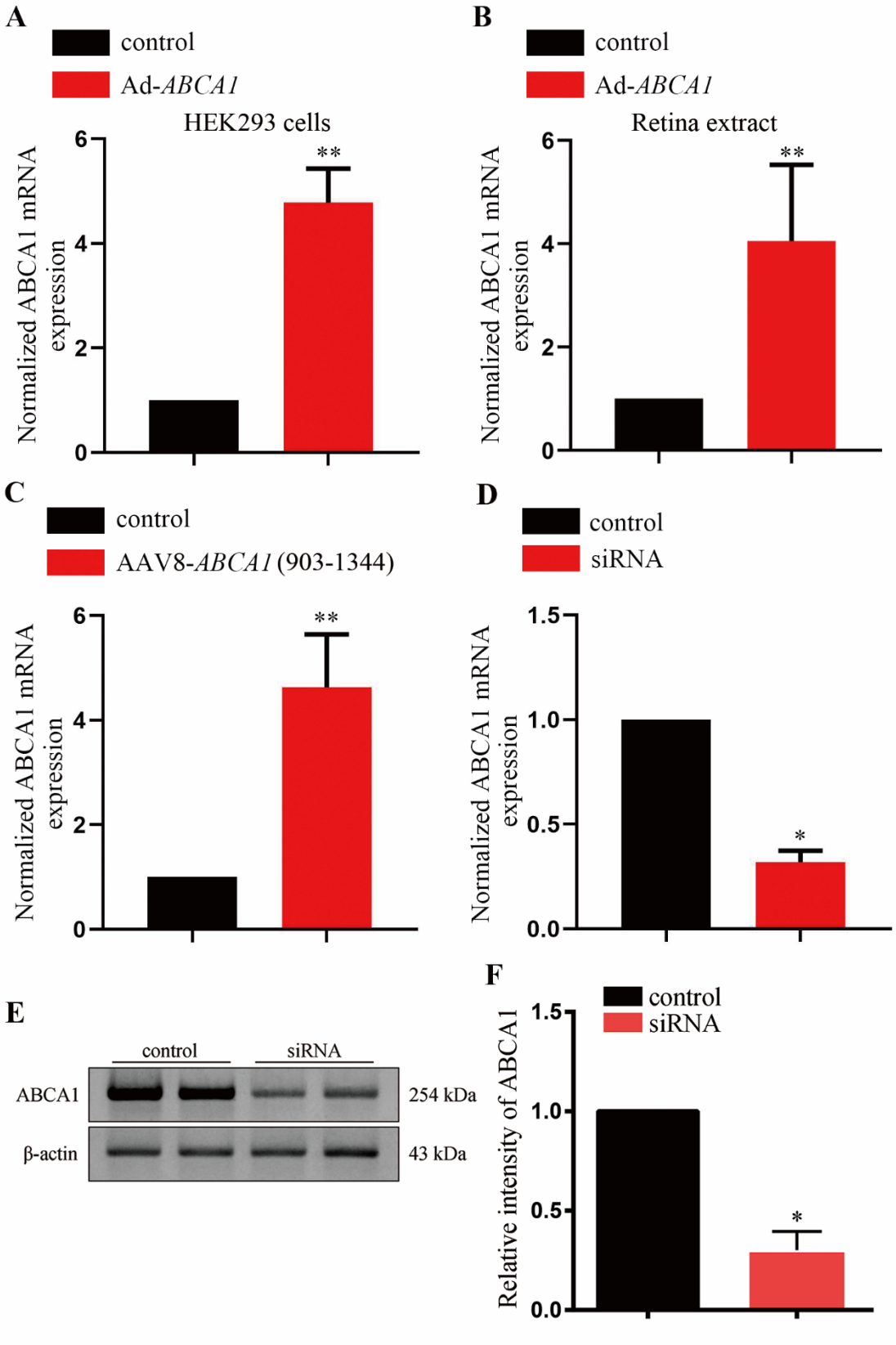

Supplementary figure 2 ABCA1 semiquantitative analysis. (A) qPCR results for ABCA1 mRNA expression from HEK293 cells after Ad-ABCA1 infection. The data of

three independent experiments expressed as the means ± S.D. **P < 0.01, unpaired Student's t-test vs control. (B) qPCR results for ABCA1 mRNA expression from retina extract after Ad-ABCA1 injection. The data of three independent experiments expressed as the means ± S.D. **P < 0.01, unpaired Student's t-test vs control. (C) qPCR results for ABCA1 mRNA expression from retina extract after AAV8-ABCA1 (903-1344) injection. The data of three independent experiments expressed as the means ± S.D. **P < 0.01, unpaired Student's t-test vs control. (D) Statistical analysis of ABCA1 mRNA expression in HEK293 cells. The data of three independent experiments expressed as the means ± S.D. *P < 0.05, unpaired Student's t-test vs control. (E) Western blot analysis showing the expression of ABCA1 after ABCA1 siRNA treatment. (F) Statistical analysis of (E), *P < 0.05, compared with control, unpaired Student's t-test vs control.

Supplementary figure 3

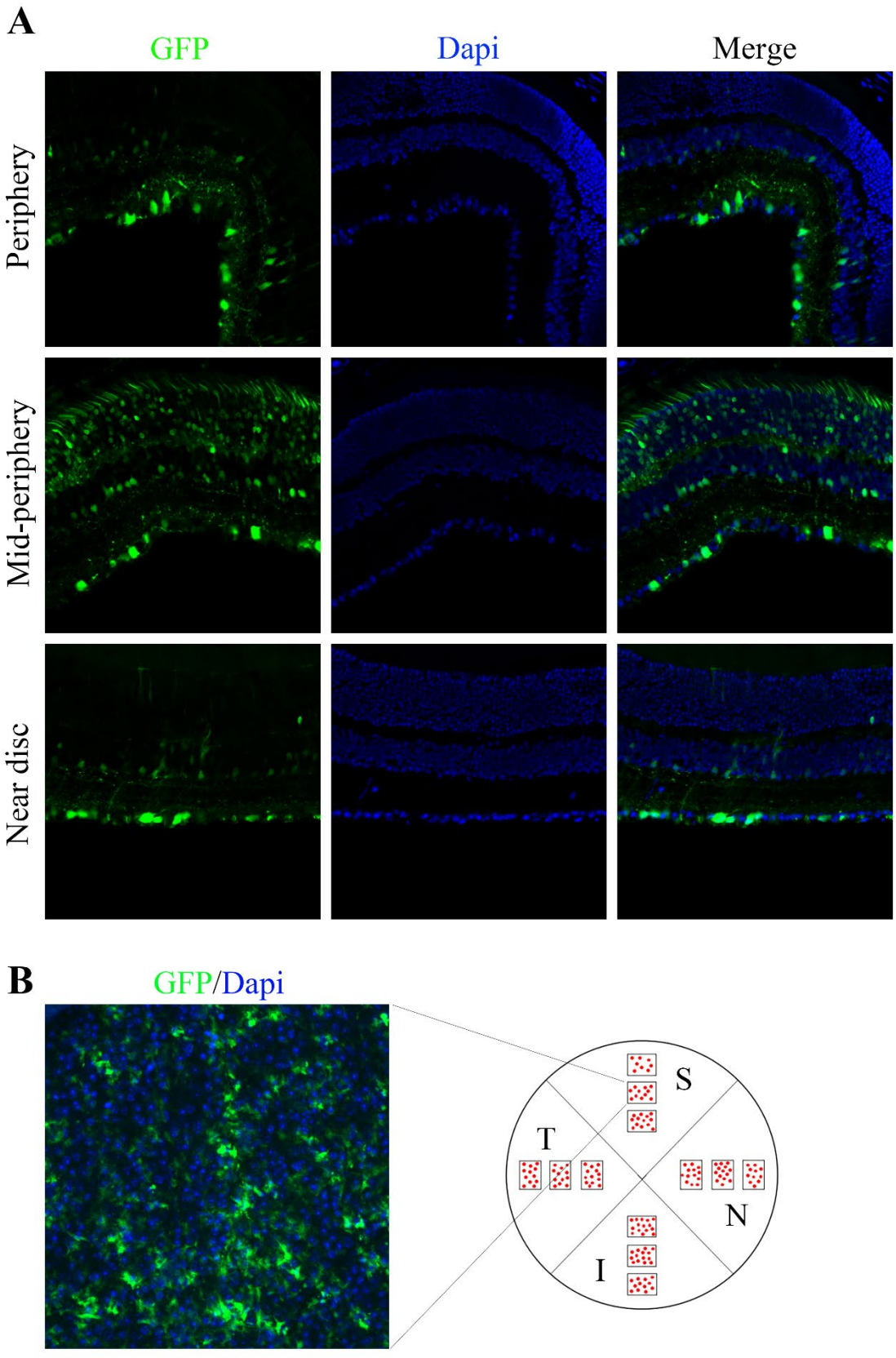

Supplementary figure 3 The representative images for Ad-ABCA1 infection. (A)

Representative immunofluorescence images of GFP expression on c-section retina slice.

(B) Representative immunofluorescence images of GFP expression on flat mount of retina.

Supplemental Methods

Quantitative RT-PCR

Total RNA was extracted using TRIzol reagent (Invitrogen), and 1 μg RNA was reverse transcribed. qRT-PCR was performed on an ABI StepOne Plus using SYBR Green ® Premix Ex Taq (Takara, Tokyo, Japan). The qPCR data were shown as relative mRNA expression versus control group. The results showed the fold-change (2-delta /delta Ct) of relative expression versus control group (-delta /delta Ct = -{sample (CT gene-CT actin)- con(CT gene-CT actin)}). For mRNA, the gene expression was normalization to β-actin.

Sequences of primers for qPCR:

Human Actin forward: TGGCACCCAGCACAATGAA

Human Actin reverse: CTAAGTCATAGTCCGCCTAGAAGCA

Human ABCA1 forward: GCTGGTGTGGACCCTTACTC

Human ABCA1 reverse: GCAGCTTCATATGGCAGCAC

Human ABCA1 (fragment 903-1344) forward: GCTGGTGTGGACCCTTACTC

Human ABCA1 (fragment 903-1344) reverse: GCAGCTTCATATGGCAGCAC

SD-OCT analysis

The OCT scanner has optical axial resolution of 7 μm, digital resolution of 3.5 μm, scan depth of 1.8 mm, and scan rate of 40 kHz. All animals were measured rapidly following anesthesia and pupillary dilation. We applied lubricating eye drops over the mouse eyes and covered them with custom-made contact lenses to prevent ocular surface issues. For imaging, animals were placed on an adjustable platform, and the camera was aligned perpendicular to the animal directly in front of and very close to the eye using a three-dimensional micromanipulator. Once the optic disc was centered and in focus using infrared imaging, we performed the circular scan (scan angle 12°) using the enhanced depth imaging (EDI) and high-resolution mode, with each B-scan consisting of 1536 A-scans centered around the optic disc. We averaged 16 frames per B-scan. We also performed posterior pole scans (scan angle 30°×25°) using EDI in high-speed mode, with each two-dimensional B scan consisting of 768

A-scans, average 9 frames per B-scan; and 25 line scans (scan angle 25°×15°) in high resolution mode, average 16 frames per B-scan. Only images with adequate signal strength index were saved and used for analysis. All OCT scans were performed by one investigator to maximize consistency, and the best image from each eye was selected for segmentation.

Viral vectors transduction in vitro

The HEK293 cells were used to transfected with Ad-ABCA1. The MOI for Ad vector was 50 genome copies (GC)/cell, incubated the virus at 37°C for 4 h, then replaced the medium with virus-free medium, and analyzed the results 48 h post-infection with ABCA1 qPCR detection. Human ABCA1 siRNA obtained from Thermo Fisher (Assay ID 107728, Catalog #AM16708, Shanghai, China). The siRNA transfection protocol was according to transfection reagent manufacturer's instructions. Briefly, in the 24-well plate, 10000-15000 HEK293 cells per well were cultured in 0.5 ml of complete growth medium 24 h prior to transfection. 40 ul of serum free medium, 4.5 ul of transfection reagent and 30 nM of siRNA were used as transfection complexes. Then we incubated the HEK293 cells with transfection complexes at 37°C for 48 h and analyzed the results with ABCA1 qPCR detection.